J. Fluid Mech. (1997), *vol.* 331, *pp.* 107–125

Turbulent flow normal to a triangular cylinder

By D. K. HEIST† AND F. C. GOULDIN
Sibley School of Mechanical and Aerospace Engineering, Cornell University,
Ithaca, NY 14853, USA

(Received 13 January 1994 and in revised form 31 May 1996)

Laser Doppler Velocimetry (LDV) measurements are presented for a nominally two-dimensional constant-density flow over a surface-mounted triangular cylinder. The thickness of the boundary layer approaching the triangular cylinder is much less than the height of the triangle. Momentum and turbulent kinetic energy balances are presented and comparisons are made with other separated and reattaching flows. Also, time domain information is presented in the form of autocorrelations and spectra. From the energy balances, the importance of the pressure transport term at the high-speed edge of the shear layer is seen. Observations of the relationships between the shapes of the spectra and the details of the energy balance are made. For example, the slope of the velocity spectra varies from the free-stream value of $-5\}3$ to a value of -1 in the middle of the recirculation region. Concurrent with this increase in slope is a decrease in the role of shear production in the turbulent kinetic energy balance and an increase in the role of advection and turbulent transport. From the two-component LDV measurements, a very low-frequency unsteadiness is shown to contribute energy preferentially to different components of the velocity fluctuations depending on the location in the flow.

1. Introduction

Turbulent separated and reattaching flows are important in many industrial and environmental situations. Incinerators, dump combustors, and engine inlets often contain step changes in the wall boundaries which may cause separation. Even smoothly varying surfaces such as those found on airfoils or in diffusers may contain areas of separated and reattaching flow. External flows responsible for the dispersion of pollutants over hills and the wind forces on buildings may also be strongly influenced by the presence of a separated region.

In these complex turbulent flows there are many different competing physical processes. In general, the separation process creates a shear layer that curves toward a bounding surface where reattachment takes place. The shear layer and the wall form the boundaries of a region of turbulent reversed flow which is re-entrained by the shear layer. The stabilizing effect of the curvature of the shear layer competes with the increase in the turbulence level due to the re-entrainment of highly turbulent reverse flow. Also, the turbulent transfer of momentum into the recirculation region counters the adverse pressure gradient in the downstream half of the recirculation region. These separated and reattaching flows present a challenge to turbulence modellers because they contain such a wide variety of important physical processes occurring in the same flow.

† Present address: Department of Mechanical Engineering, University of Surrey, Guildford, Surrey GU2 5XH, UK.

Many different flows that come under the general heading of separated and reattaching flows have been the subject of investigation. Notable studies include separated boundary layers (e.g. Dianat & Castro 1991; Simpson 1981), flow over a backward-facing step (e.g. Chandrsuda & Bradshaw; Driver & Seegmiller 1985), flow over a normal flat plate (e.g. Ruderich & Fernholz 1986; Castro & Haque 1987) and flow over obstacles submerged in turbulent boundary layers (e.g. Arya, Capuano & Fagen 1987; Atli 1988). These flows share many common characteristics, beginning with the basic structure: a region of reverse flow bounded on one side by a shear layer and on the other by a wall.

One feature often observed in these flows is a steady rise with downstream distance in the maximum turbulent kinetic energy and Reynolds shear stress at each streamwise location when normalized by the square of the local velocity difference across the shear layer (Ruderich & Fernolz 1986; Castro & Haque 1987; Dianat & Castro 1991). Just before reattachment the Reynolds stress is usually seen to begin to decrease. Although the decrease is initially rapid, Chandrsuda & Bradshaw (1981) found for the backward-facing step that to achieve the lower values of turbulent kinetic energy and shear stress typical of a turbulent boundary layer, a very long redevelopment length was required following reattachment.

The near-wall layer in the recirculation region has been observed not to follow the log-law for a turbulent boundary layer (Ruderich & Fernholz 1986; Adams & Johnston 1988), but instead to exhibit characteristics of a 'laminar-like' boundary layer (Castro & Haque 1987). Although large velocity fluctuations are present, values of the Reynolds shear stress are too low to form the normal turbulent boundary layer structure. The skin friction measurements and mean velocity profiles of Adams & Johnston (1988) suggest a flow in which the near-wall shear stress is predominantly viscous. For example, the skin friction coefficient was observed to vary approximately with the Reynolds number to the $-\frac{1}{2}$ power, consistent with the idea of a laminar-like boundary layer.

A third feature common to many separated and reattaching flows is periodicity in the shear layer much like that found by Winant & Browand (1974) for the free mixing layer. In that study, vortical structures were observed using dye injected into the interface between the two streams. The frequency (non-dimensionalized by the vorticity thickness and the mean velocity in the shear layer) at which these structures occurred was 0.2. For the flow over the backward-facing step, Driver, Seegmiller & Marvin (1983) found peaks in the pressure and velocity spectra at the same non-dimensional frequency.

Another type of unsteadiness with a very low frequency has been observed in several different separated and reattaching flows. The timescale of this motion, seen as a spectral peak, has been observed to be approximately eight times as long as it takes for the free stream to pass over the separation bubble (Castro & Haque 1987). For the flow over a backward-facing step, this motion was investigated by Eaton & Johnston (1982) who attributed this cross-stream low-frequency motion of the shear layer to an 'instantaneous imbalance between the entrainment rate from the recirculation zone and the reinjection rate near reattachment'. This very low-frequency unsteadiness has been observed in the flow over a flat plate normal to the free stream with a splitter plate attached to the downstream side (Castro & Haque 1987), the separated boundary layer (Dianat & Castro 1991; Simpson 1981), and in the flow past a thick plate parallel to the free stream (Kiya & Sasaki 1983).

In the current study, the flow over a surface-mounted triangular obstacle is examined. The triangular obstacle was chosen because of its relevance to the flow in a

municipal solid waste incinerator and in utility boilers. As was discussed in Heist, Ravichandran & Gouldin (1994), where comparisons are made between some of the results presented here and the results of computations using the standard $k-\epsilon$ model and the finite element method, the flow over a triangular obstacle exhibits many of the important features of incinerator and furnace flows. In the context of separated and reattaching flows, the flow over a surface-mounted triangular obstacle has several features that distinguish it from the flows discussed above which have received attention in the past. Unlike the separated boundary layer, the separation point in the flow over a triangular obstacle is fixed by the geometry of the wall boundaries and therefore is not expected to fluctuate. Unlike the flow over the backward-facing step, the free-stream flow is accelerated over the separation point and continues to accelerate part of the way to reattachment. Because of the geometry of the separation region, the shear layer has more curvature than the shear layer formed in the flow over a backward-facing step.

The purpose of this paper is to report experimental observations and to describe the important physical processes occurring in the flow over a surface-mounted triangular obstacle that are revealed by these observations. The two-component laser Doppler velocimetry (LDV) velocity measurements presented allow a detailed examination of momentum and turbulent kinetic energy balances for two regions in the flow. The two regions are chosen to demonstrate the difference in the flow in the forward part of the recirculation and the flow closer to reattachment. Also, time domain information for the recirculation zone, which is difficult to measure is presented in the form of spectra. Observations of the relationships between the shapes of the spectra and details of the turbulent kinetic energy balance are made.

In §2 the experimental apparatus and the data acquisition process are described. The mean flow field and Reynolds stresses are described in §3. Momentum balances, turbulent kinetic energy balances, autocorrelations, and spectra are presented in §4.

2. Experiment

One motivation for this study is the desire to model certain aspects of incinerator and furnace-related flows to obtain data for comparison with numerical predictions (Heist *et al.* 1994). The first step in understanding the turbulent mixing processes in such practical flows is to study the characteristics of an isothermal flow that has similar features, in particular a geometrically induced separation region. The use of water permits a scaling which makes the size of the experimental apparatus manageable, while still achieving high Reynolds number.

2.1. *Water tunnel*

The water tunnel used in this study is a gravity-driven tunnel with pumps used to recirculate the flow. The flow system provides a steady flow through the test section which has a cross-section of 117 mm by 330 mm and a length of 1100 mm (see figure 1). The obstacle in this study is a surface-mounted triangle 38.1 mm high; it extends 58.4 mm upstream and 43.2 mm downstream of its apex and spans the width of the test section. A flow-straightening section which measures 530 mm in length is situated directly upstream of the test section. Included in this section are a diffuser and a series of screens designed to provide uniform inlet flow and low inlet turbulence levels.

The reference velocity is defined as the streamwise velocity midway between the apex of the triangle and the opposite wall at the streamwise location where separation takes place ($x\}H = 0,\ y\}H = 2.04$); the reference velocity was maintained at 0.60 m s^{-1}

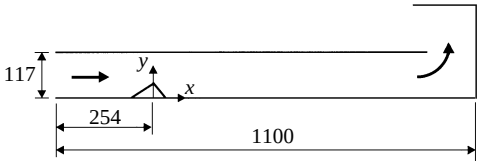

FIGURE 1. Test section geometry. All dimensions in mm.

during the experiments. DeBroderode & Bradshaw (1972) recommend a spanwise aspect ratio of at least 10 for two-dimensionality of the flow away from the sidewalls; more recent work (Hancock & Castro 1993) suggests that an aspect ratio of at least 20 is required form non-negligible sidewall effect. Although the spanwise aspect ratio of the obstacle is somewhat low in the present experiment ($H\}\text{span} = 9$), the spanwise variation in the mean inlet velocity (four step heights upstream of separation) is less than about 3 % of the reference velocity over the middle 90 % of the chamber. Another check on the two-dimensionality of the flow is made by finding the volume flow rate per unit span at each streamwise measurement station by integrating the mean velocity profiles. It is found that the volume flow rate per unit span along the centre (where the reported measurements are taken) varies less than 5 % throughout the entire measurement domain.

The Reynolds number based on triangle height (H) and reference velocity (U_{ref}) is 2.8×10^4 for the measurements reported here. The average inlet turbulent kinetic energy non-dimensionalized by U_{ref}^2 (at $x\}H = 0$) is 3.58×10^{-4} and the flow rate per unit span is 0.0487 $m^2\ s^{-1}$. The turbulence level relative to the reference velocity at the streamwise location where separation takes place is approximately 1.5 % and exhibits the usual $-5\}3$ slope in the power spectrum.

The boundary layer thickness ($\delta_{0.99}$) is less than $\frac{1}{40}$ of the obstacle height at the separation point on the triangular obstacle. Owing to data acquisition difficulties near the wall it was not possible to measure detailed boundary layer profiles. However, the flow is accelerated over the triangle to such an extent that Moretti & Kays's acceleration parameter is much greater than the critical value required for relaminarization (Moretti & Kays 1965). This suggests that the separation boundary layer is therefore laminar, although the free-stream turbulence is not negligible.

2.2. *Data acquisition and analysis*

Detailed two-component velocity measurements are taken with laser Doppler velocimetry (LDV) using the 488.0 and 514.5 nm lines from a 4 W argon–ion laser. The beam splitting, frequency shifting, and coupling of laser light to fibre-optic cables are all accomplished using a Colorburst™ Multicolor Beam Separator (TSI, Inc. Model 9201). The LDV system is used in the fringe mode with frequency shifting by 40 MHz to eliminate directional ambiguity in the velocity measurements. The measurement volume has a diameter of approximately 80 μm and a length in the spanwise direction of about 1 mm. The measurement volume is translated with a three-dimensional traversing system that has a positioning accuracy of at least 0.1 mm for 1 m of travel in each direction. The accuracy of the alignment of the LDV measurement volume relative to the water tunnel is within ± 0.1 mm in each direction.

Light scattered from silicon carbide seed particles (1–3 μm nominal diameter) is collected in backscatter. The signals from the photomultiplier tubes are downmixed to either 20 kHz or 200 kHz, depending on the value of the mean velocity. These downmixed signals are processed using TSI model 1990B counter processors, which measure the time required for 16 cycles of a Doppler burst with a resolution of 1 ns.

At least 2500 velocity samples are taken at each measurement station with a sampling rate that ranged from about seven samples s^{-1} in the recirculating region to about 25 samples s^{-1} in the free stream (much slower than the LDV data rate, see later). These measurements are used to compute mean velocities, Reynolds stresses and triple products. To compute the autocorrelation function, Mayo's (1978) discretized lag products technique is used. Twenty-five sets of 10000 points are recorded along with the time between data points to be used in the time series analysis.

In §4, where momentum and turbulent kinetic energy balances are presented, the necessary cross-stream derivatives are obtained using b-spline coefficients of an approximation to the measured profile. For derivatives in the streamwise direction, three-point central differencing is used.

2.3. *Uncertainties*

Statistical uncertainties in the sample mean and standard deviation are estimated assuming that the velocity is a normally distributed random variable. Of the 2500 samples used in calculating means and moments, at least 670 are independent samples because the data were recorded somewhat faster than once every two integral timescales. With this number of independent samples the true mean velocity is estimated to be within at most $\pm 0.076\,s$ of the sample mean with 95% confidence, where s is the sample standard deviation. The true standard deviation is within at most $\pm 5\%$ of the sample velocity standard deviation with 95% confidence, and the true third moments are estimated to be within $0.095s^3$ of the sample third moments (Castro 1989). In figure 2(*a*), error bars show the worst-case statistical uncertainty on the mean and standard deviation of the streamwise velocity three step heights downstream of the separation point. Although triple products are not discussed separately below, the triple-product data are used in the turbulent kinetic energy balance. Therefore, a representative profile of $\overline{ku}$ (defined as $\frac{1}{2}(\overline{u^3}+\overline{uv^2})$) is shown with error bars in figure 2(*b*).

The errors in the Reynolds shear stress measurements were minimized by ensuring that the seeding density was low enough that on average only one particle was in the measurement volume at a time. This helps to ensure that both components of velocity were measured from the same seed particle, which eliminates any problems with lack of spatial correlation in the spanwise direction corrupting the data.

LDV errors can be classified in four main categories: particle tracking errors, bias errors, instrumentation errors, and broadening mechanisms (Miles 1991). To control tracking errors, the seed particles used to scatter laser light must have a sufficiently high frequency response to the velocity fluctuations in the flow. Following the analysis in Drain (1980), one finds that at a frequency of 500 Hz the amplitude of the variation of the velocity of the seed particle will equal that of the fluid to within 1%, if the particles are smaller than 12 μm in diameter. That frequency is higher than the highest frequencies seen in the flow and the seed particles used are an order of magnitude smaller than the required diameter. The settling velocity of the silicon carbide seed particles is 1.2 mm s^{-1}, much smaller than any velocity of interest in this study. Velocity bias errors occur when the rate at which data are recorded is correlated with the velocity of the particles. This correlation leads to faster sampling when the velocity fluctuates above the mean velocity and slower sampling when the velocity fluctuates below the mean. This type of sampling would record a larger number of particles moving faster than the mean velocity than the number of particles moving slower than the mean velocity; calculating the mean from these samples would produce an estimate of the mean velocity that is based above the true mean. In the present study, the

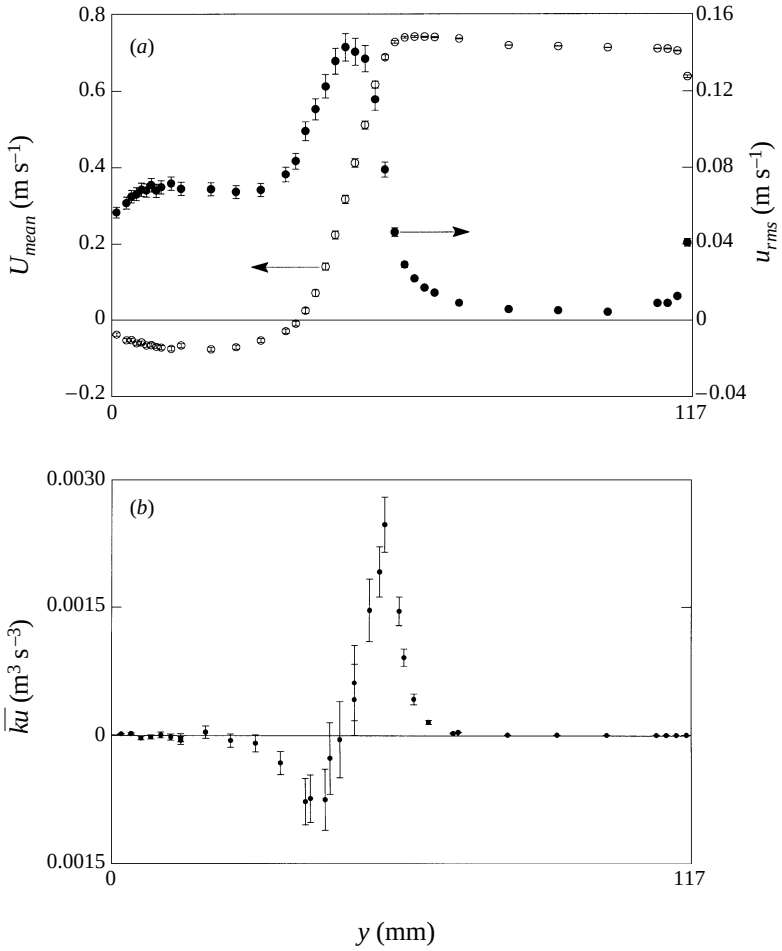

FIGURE 2. Estimated error bars on (*a*) mean (○) and r.m.s. (●) velocities and (*b*) triple products due to statistical uncertainty. $x\}H = 3$.

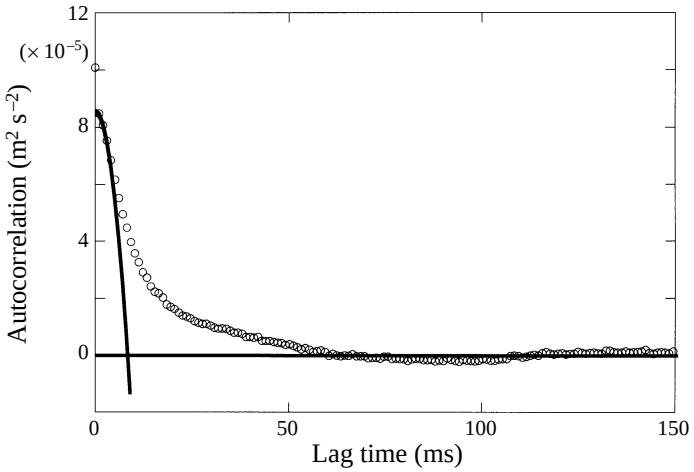

FIGURE 3. Autocorrelation function showing noise spike at the origin. $y\}H = 2.1$, $x\}H = -4$. ○, Autocorrelation estimates; ——, parabolic fit near the origin.

sampling rates used in taking data for mean velocities and higher-order moments are much lower than the validated signal rate. Therefore, the recorded data are spaced nearly equally in time, and quantities free of velocity bias are obtained (Stevenson, Thompson & Roesler 1982).

The instrumentation errors rise from the finite timer resolution in the counter processors and from skewed zero crossing in the Doppler burst due to nonlinear filter phase delay. Both of these errors are expected to be uncorrelated from one measurement to the next and will be discussed below. Broadening mechanisms consist of gradient broadening and phase noise, which both tend to broaden the velocity p.d.f. and thus lead to an overestimation of the r.m.s. velocity. These errors are also uncorrelated between measurements and will be discussed below.

In the high-velocity part of the flow, where the turbulence levels are very low, the uncorrelated noise in the signal leads to an overestimation of the turbulence level. This uncorrelated noise can result from phase noise, gradient broadening, instrumentation errors due to timing resolution, and skewing of the Doppler-signal zero crossings via the filtering process (Miles 1991). Fortunately, the degree of overestimation of the velocity variance can be determined from the velocity autocorrelation, where the uncorrelated noise appears as a spike added to the autocorrelation function at the origin. To correct for this noise, the autocorrelation was computed and then extrapolated to the origin (time lag = 0) to find the true value of the velocity variance as suggested by Whiffen, Lau & Smith (1978). A typical example is shown in figure 3 for a location upstream of separation at $x\}H = -4$, $y\}H = 2.1$. For low turbulence levels, since the autocorrelation function is expected to be parabolic near $\tau = 0$, a least-squares parabolic fit to the first few data points is used to extrapolate to find the velocity variance. In the shear layer and the recirculation region where the turbulence level is relatively high, the uncorrelated noise in the velocity signal was found to be negligible, and therefore no correction is made to those data.

3. Mean flow and Reynolds stresses

3.1. *Mean flow*

The reattachment length (L_r) is widely regarded as the most important parameter characterizing separated and reattaching flows (Eaton & Johnston 1981; Simpson 1985; Thangam & Speziale 1992). The behaviour of the reattachment length as a function of Reynolds number is used to define different regimes of flow – laminar, transitional, and turbulent (Armaly *et al.* 1983). The turbulent regime is characterized by a reattachment length which is independent of Reynolds number. The reattachment length in this study is estimated by extrapolating to the wall the locus of points where the mean streamwise velocity is zero. This technique is discussed in detail by Westphal, Johnston & Eaton (1984). Figure 4 shows the variation of the reattachment length (normalized by the obstacle height) with the Reynolds number for the present geometry. In the backward-facing step and obstacle flows, this curve usually shows a dramatic decrease of the reattachment length with increasing Reynolds number in the transitional regime (not measured in the present case), followed by a gradual rise and levelling off of the reattachment length in the turbulent regime (Armaly *et al.* 1983; Atli 1988). Comparison of this behaviour with figure 4 indicates that the present measurements ($Re = 2.8 \times 10^4$) are made in the turbulent, Reynolds-number-independent regime.

The mean velocity profiles are shown in figure 5. The free stream accelerates past the nose and continues to accelerate to about three step heights downstream of separation.

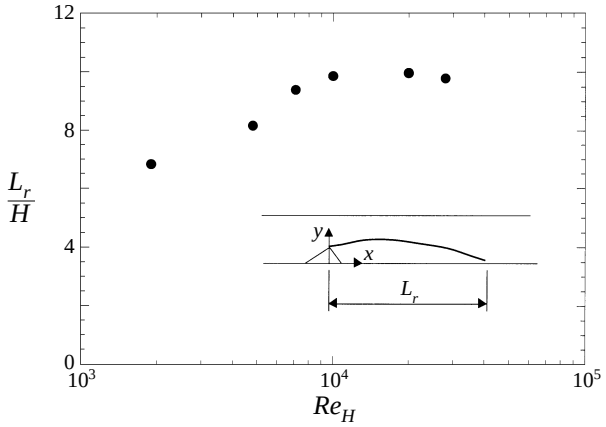

FIGURE 4. Reattachment length (non-dimensionalized by obstacle height) *vs.* Re_H.

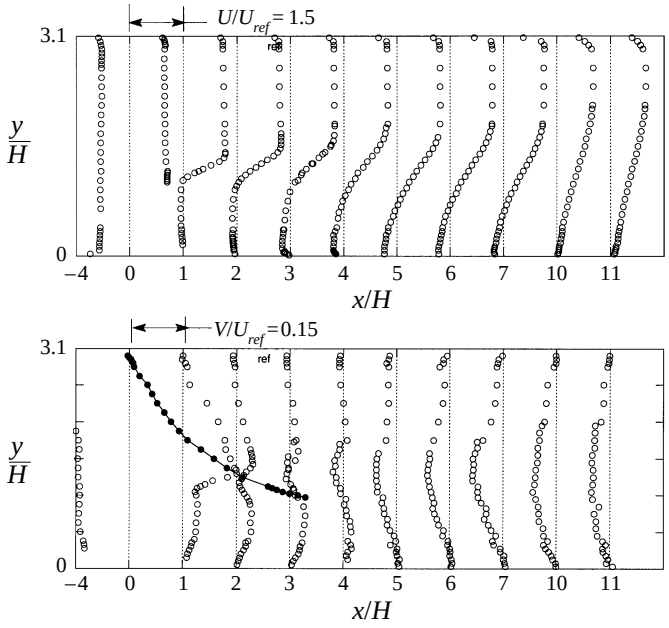

FIGURE 5. Mean velocity profiles normalized by the reference velocity.

The shear layer created in this separation process is at first very narrow but spreads in the downstream direction. The recirculation region extends 9.8 step heights downstream of the apex of the triangular obstacle. The cross-stream velocity profiles in figure 5(*b*) show that the cross-stream velocity changes direction between the forward part of the recirculation zone and the downstream part.

The streamlines shown in figure 6 were obtained by integrating the mean velocity profiles outward from the wall on which the triangular obstacle is mounted. This whole-field view of the flow demonstrates the consistency of the measurements.

The thickness of the shear layer is quantified using the vorticity thickness,

$$\Lambda = \frac{\Delta V}{(\text{¥}V\}\text{¥}x)_{max}}, \tag{1}$$

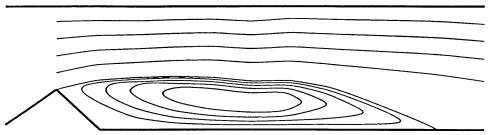

FIGURE 6. Streamlines. The streamfunction values (non-dimensionalized with H and U_{ref}) are incremented by 0.0306 from -0.0306 to -0.1225 in the recirculation zone and incremented by 0.418 from 0 to 2.09 in the free stream.

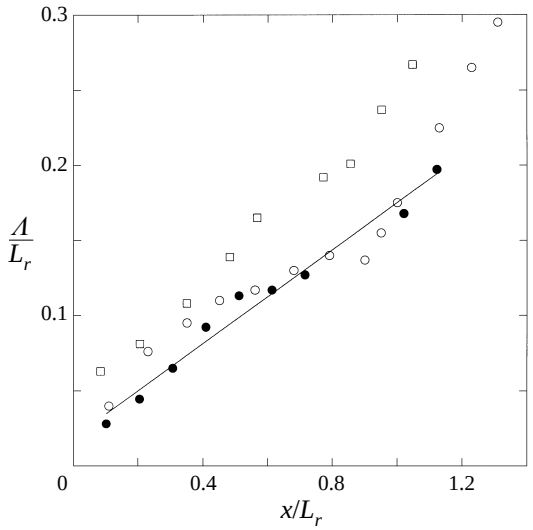

FIGURE 7. Vorticity thickness *vs.* downstream distance: ●, present results; ——, linear fit to present data for comparison; ○, Dianat & Castro (1991); □, Castro & Haque (1987).

and its variation with downstream distance is shown in figure 7. The velocity difference across the shear layer, ΔV, is equal to the magnitude of the maximum reverse velocity plus the maximum downstream velocity at a given streamwise location. Also shown in the figure are a linear fit to the present data, and results from the flow over a fence (Castro & Haque 1987) and a separated boundary layer flow (Dianat & Castro 1991). The spreading rate for a plane mixing layer is known to be linear with downstream distance, although poor agreement on the rate is found in the literature (Mehta & Westphal 1986). It can be seen that although the present vorticity thickness growth rate is not far from being linear, there is a significant decrease in the growth rate midway to the reattachment point followed by an increase very near reattachment. This behaviour can also be seen for the flow over a fence.

3.2. *Reynolds stresses*

Streamwise and cross-stream normal Reynolds stresses in the (x, y)-plane are shown in figure 8. The streamwise stress profile has a peaked shape, while the cross-stream stress profile is more rounded. As will be shown later, in the Reynolds stress equations the generation term is much larger for the streamwise normal Reynolds stress than it is for the cross-stream stress. The peak values of the measured streamwise stress are approximately twice the corresponding peak cross-stream values, as can be seen from the structure parameter $\overline{u^2}\}\overline{v^2}$ in figure 9. This ratio remains approximately constant throughout the domain measured. Also shown in figure 9 is the development of $\overline{u^2}\}\overline{v^2}$ in the free stream at $y\}H = 2.1$. The high values near the separation point are caused by the contraction of the flow as it accelerates over the triangular obstacle. This

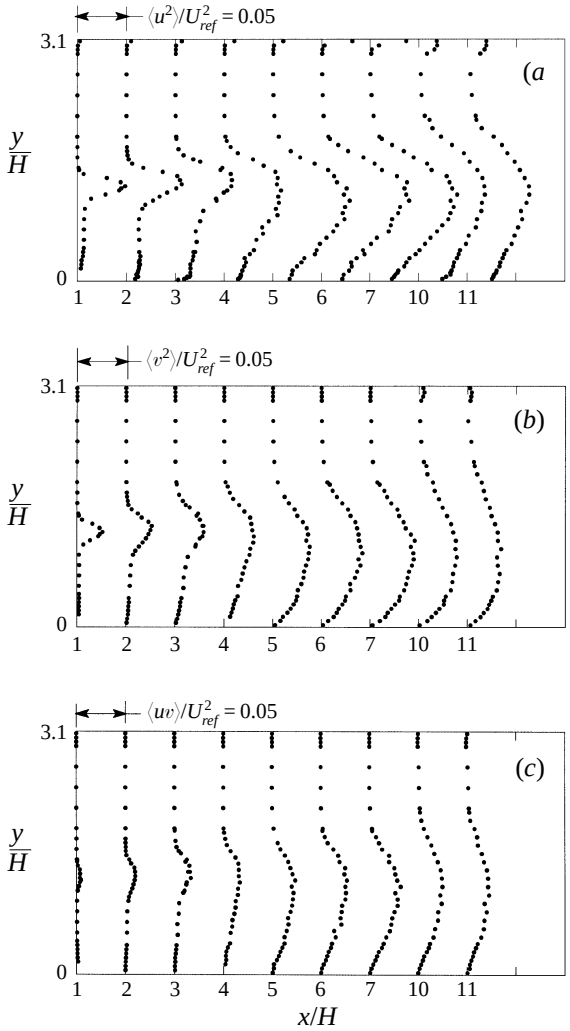

FIGURE 8. Reynolds stress profiles normalized by the square of the reference velocity. (*a*) $\overline{uu}\}V_{ref}^2$, (*b*) $\overline{vv}\}V_{ref}^2$, (*c*) $-\overline{uv}\}V_{ref}^2$.

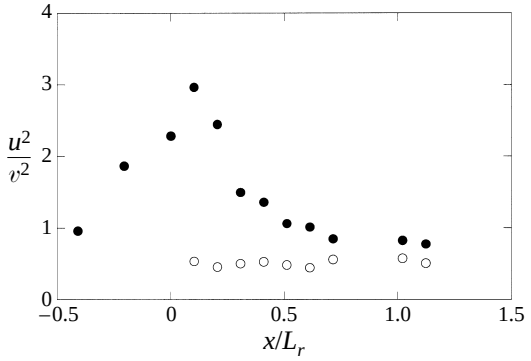

FIGURE 9. Structure parameter $\overline{uu}\}\overline{vv}$: ○, at the location of maximum kinetic energy; ●, at $y\}H = 2.1$.

structure parameter decreases as the free stream expands downstream of the separation points.

The Reynolds shear stress is shown in figure 8(*c*). The shear stress is negative throughout the measurement domain, consistent with gradient transfer in almost all regions of this flow. However, in the near-wall region of the recirculation zone close to the separation point there is a region of counter-gradient turbulent transport.

In each of the Reynolds stress components, a noticeable change in the slope (e.g. $\partial\overline{u^2}/\partial y$) on the low-speed side of the shear layer is seen in the profiles near separation ($x/H = 1, 2$ and 3). The flatness of the profiles nearer the wall suggests that the turbulence in this region is not created locally, nor transported from the shear layer. This phenomenon is present in the flow over a normal plate as measured by Castro & Haque (1987), who speculate that the turbulence is likely to originate from the reattachment region. This point will be addressed again in §4.2, where turbulent kinetic energy balances are presented.

4. Derived quantities

In §§4.1 and 4.2 momentum and turbulent kinetic energy balances are presented for two regions, one in the forward part of the separation region ($x/H = 2$) and one closer to reattachment ($x/H = 6$). These two positions were chosen to demonstrate the difference in behaviour that the direction of the cross-stream flow makes in the balances.

4.1. *Momentum balance*

The streamwise Reynolds-averaged momentum equation for a steady constant-density flow in the x-direction is

$$\frac{\partial U}{\partial t} = -U\frac{\partial U}{\partial x} - V\frac{\partial U}{\partial y} - \frac{1}{\rho}\frac{\partial P}{\partial x} - \frac{\partial \overline{u^2}}{\partial x} - \frac{\partial \overline{uv}}{\partial y} = 0, \tag{2}$$

where the viscous terms have been neglected. Each term in the equation except the pressure gradient is estimated from the LDV data presented above as discussed in §2.2. The pressure gradient is found by balancing the equation. Momentum balances are presented in figure 10.

At $x/H = 2$, the free-stream flow is still accelerating from the contraction imposed by the triangular obstacle. Figure 10(*a*) shows a favourable pressure gradient in the free stream which is balanced by the streamwise advection term. The Reynolds shear stress transports momentum from the high-velocity free stream to the low-velocity recirculating region. Cross-stream advection is moving fluid away from the wall toward the free stream carrying x-momentum with it. Since the cross-stream is moving from an area of lower-momentum fluid to higher-momentum fluid, this is seen as a loss of x-momentum in the shear layer.

At $x/H = 6$, several of the terms in the balance have reversed their signs. For example, figure 10(*b*) shows an adverse pressure gradient working to decelerate the flow. It is this adverse pressure gradient that causes the slower-moving fluid to begin to move backwards in the recirculation region. In the free stream, the pressure gradient is again balanced by the streamwise advection term. The shape of the shear stress term is similar at $x/H = 2$ and 6, showing a loss of momentum on the high-velocity side of the shear layer and a gain on the low-velocity side. Contrary to the situation near separation, cross-stream advection moves fluid away from the free stream toward the wall, from an area of higher momentum to lower momentum. Therefore, as seen in figure 10(*b*), cross-stream advection represents an increase in x-momentum.

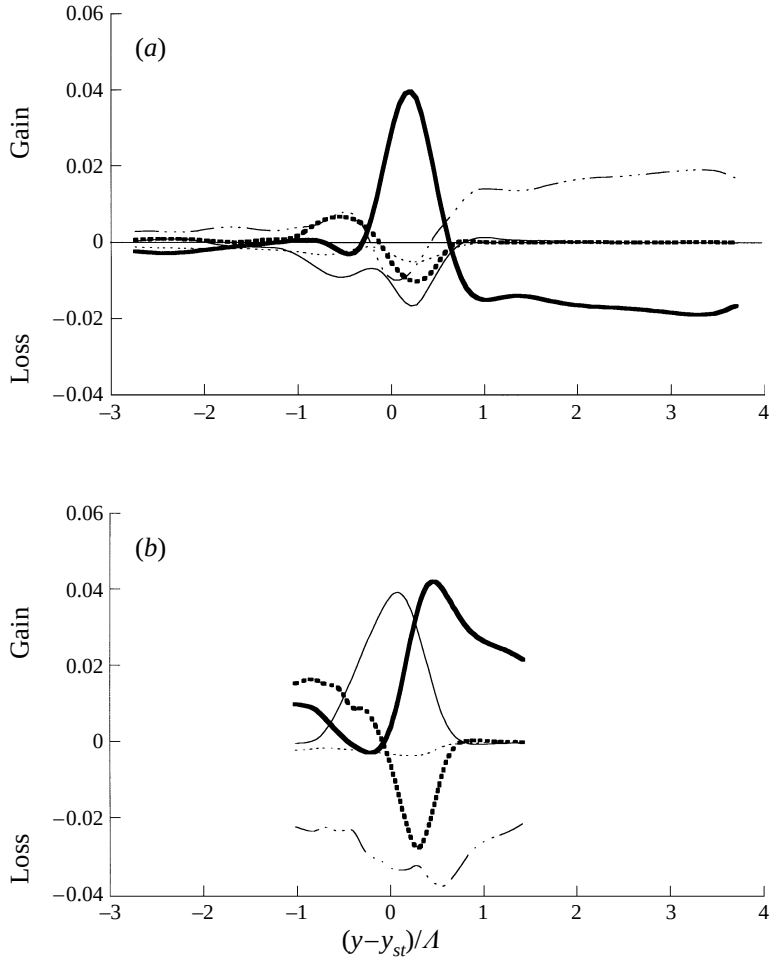

FIGURE 10. Momentum balances: (*a*) $x/H = 2$, (*b*) $x/H = 6$. ——, $-U\partial U/\partial x$; ——, $-V\partial U/\partial y$; **-----**, $-\partial\overline{uv}/\partial y$; -----, $-\partial\overline{u^2}/\partial x$; —·—·—, $-(1/\rho)\partial P/\partial x$. Ordinate is non-dimensionalized with ΔV and Λ, the shear layer thickness; y_{st} is the value of y on the separation streamline.

4.2. *Turbulent kinetic energy balances*

Each term in the kinetic energy budget (Tennekes & Lumley 1972),

$$\underbrace{\frac{\partial k}{\partial t} = -U\frac{\partial k}{\partial x} - V\frac{\partial k}{\partial y}}_{\text{advection}} \quad \underbrace{-\overline{uv}\left(\frac{\partial U}{\partial y} + \frac{\partial V}{\partial x}\right)}_{\text{shear production}} \quad \underbrace{-(\overline{u^2}-\overline{v^2})\frac{\partial U}{\partial x}}_{\text{normal production}}$$

$$\underbrace{-\left[\frac{1}{\rho}\frac{\partial \overline{up}}{\partial x} + \frac{1}{\rho}\frac{\partial \overline{vp}}{\partial y}\right]}_{\text{pressure transport}} \quad \underbrace{-\frac{\partial \overline{ku}}{\partial x} - \frac{\partial \overline{kv}}{\partial y}}_{\text{turbulent transport}} \quad - \underbrace{\varepsilon}_{\text{dissipation rate}} = 0, \tag{4}$$

has been evaluated from the velocity measurements with the exception of the dissipation rate and the pressure transport term, which is commonly neglected in

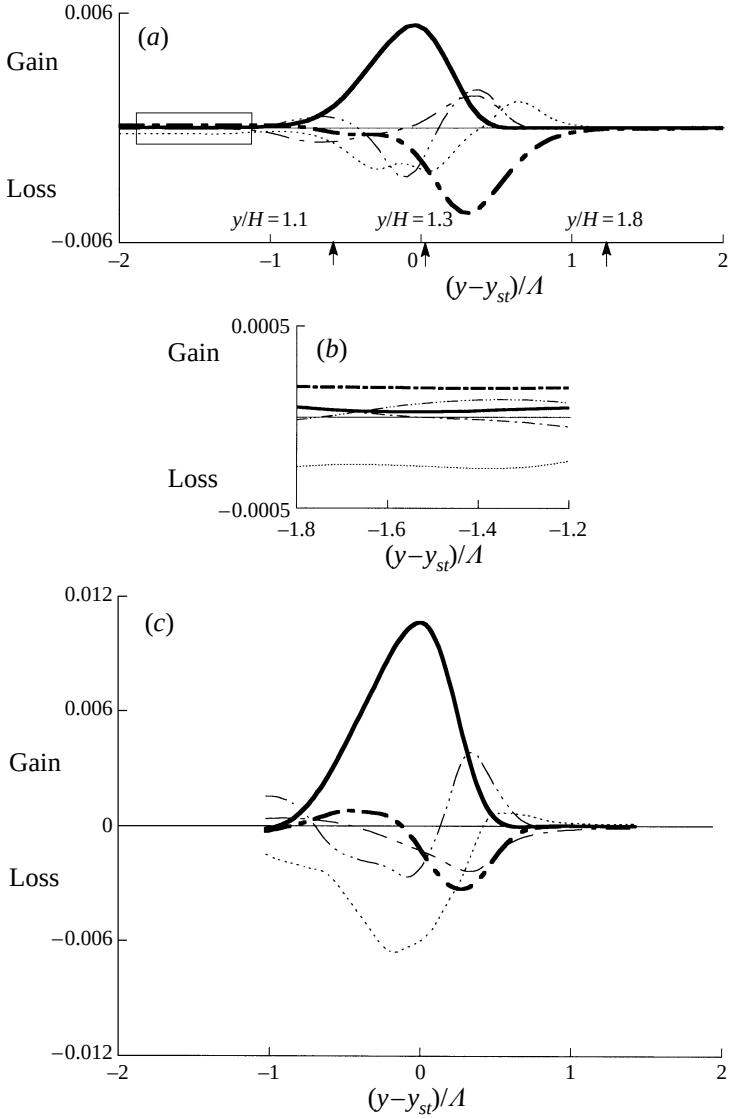

FIGURE 11. Turbulent kinetic energy balances: (*a*) $x\}H = 2$, (*b*) inset region from (*a*), (*c*) $x\}H = 6$. ——, production; —-—, streamwise advection; —·—, cross-stream advection; —---—, turbulent transport; ----, dissipation. Ordinate is non-dimensionalized with ΔV and Λ, the shear layer thickness; y_{st} is the value of y on the separation streamline.

separated and reattaching flows (Chandrsuda & Bradshaw 1981; Driver & Seegmiller 1985; Dianat & Castro 1991). By neglecting the pressure transport term, one can estimate the dissipation rate by balancing the equation. Energy balances estimated in this way are shown in figure 11 for two streamwise stations, $x\}H = 2$ and 6. The normal and shear production terms are shown together in figure 11, since the normal production term is much smaller than the shear production term. Also, since the streamwise turbulent transport term is much smaller than the cross-stream term, these terms are shown together. However, the two advection terms are presented separately to show the significance of the cross-stream advection term on the balance. The maximum magnitude of the cross-stream term is less than half that for the streamwise

term; however, it is of the same order as the turbulent transport term. As seen for the momentum balance, the effect of cross-stream advection in the energy balance is opposite at $x/H = 2$ and 6. Near reattachment both advection terms are acting to decrease the turbulent kinetic energy on the high-velocity side of the shear layer; near separation, however, the cross-stream term is acting to increase turbulent kinetic energy while the streamwise term is reducing it.

In §4.1, it was remarked that the turbulence on the low-speed side of the flow near separation appears as if it were not created locally. An expanded view of the turbulent kinetic energy balance in this region is shown in figure 11(*b*). Indeed, this figure suggests that the major source of turbulence in this region is streamwise advection from the downstream part of the separation bubble.

The dissipation rate estimates in figure 11 show a gain of energy near the edge of the high-speed side of the shear layer. This unphysical result has also been seen by Dianat & Castro (1991) for the separated boundary layer on both the high- and low-speed sides of the shear layer. Estimates of dissipation rate from spectra which exhibit an inertial subrange can be made for $(y-y_{st})/\Lambda$ (where y_{st} is the value of y on the separation streamline) greater than about 1 using the one-dimensional Kolmogorov constant found by Boston & Burling (1972). At $x/H = 2$, for $(y-y_{st})/\Lambda = 1.25$ this estimate of the dissipation rate is approximately two orders of magnitude less than the streamwise advection term. In the present results, especially noticeable at $x/H = 2$, the streamwise advection term is the only other non-zero term shown in the balance at the edge of the shear layer. Therefore, the source of the unphysical result is either uncertainty in the estimate of streamwise advection or the importance of the neglected pressure term. A conservative estimate of the uncertainty in the streamwise advection term is $\pm 15\%$, based on the expected error in the mean velocity and turbulent kinetic energy. Since this uncertainty is too small to account for the 'negative' dissipation rate, it seems likely that the pressure transport term is not negligible in this flow, approximately balancing streamwise advection on the high-velocity side of the shear layer. The pressure transport term may be more important in both the present flow and the flow studied by Dianat & Castro (1991) than in flow over the backward-facing step, because of the increased streamline curvature in these flows; energy transfer through the pressure–velocity correlation term is known to be appreciable in flows with streamline curvature (Townsend 1976).

The generation term from the Reynolds stress equations for the two components of the normal Reynolds stresses measured in this study are

$$G(\overline{uu}) = -\overline{uu}\frac{\partial U}{\partial x} - \overline{uv}\frac{\partial U}{\partial y}, \quad G(\overline{vv}) = -\overline{uv}\frac{\partial V}{\partial x} - \overline{vv}\frac{\partial U}{\partial x}. \tag{5}$$

These are plotted in figure 12. The generation of $\overline{vv}$ is almost negligible compared to the generation of $\overline{uu}$ since $\partial U/\partial y$ is by far the largest velocity gradient. This helps to explain why $\overline{uu}$ is approximately twice as large as $\overline{vv}$ at the cross-stream locations where the kinetic energy is a maximum (see figure 9).

4.3. *Autocorrelations and spectra*

The autocorrelation function is estimated from 25 blocks of continuous velocity data consisting of 10000 samples each, using Mayo's discretized lag products technique (Mayo 1978) as discussed in §2.2. One-sided power spectral density estimates are computed by Fourier transforming the autocorrelation function, after the autocorrelation is extended to negative lag times making use of the symmetry of the autocorrelation. Also before Fourier transforming, the autocorrelation is multiplied by

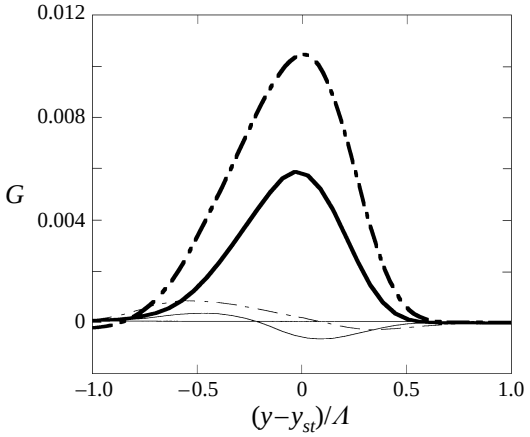

FIGURE 12. Generation of Reynolds stresses: ——, generation of $\overline{uu}$ at $x\}H = 2$; ——, generation of $\overline{vv}$ at $x\}H = 2$; —·—, generation $\overline{uu}$ at $x\}H = 6$; —··—, generation of $\overline{vv}$ at $x\}H = 6$.

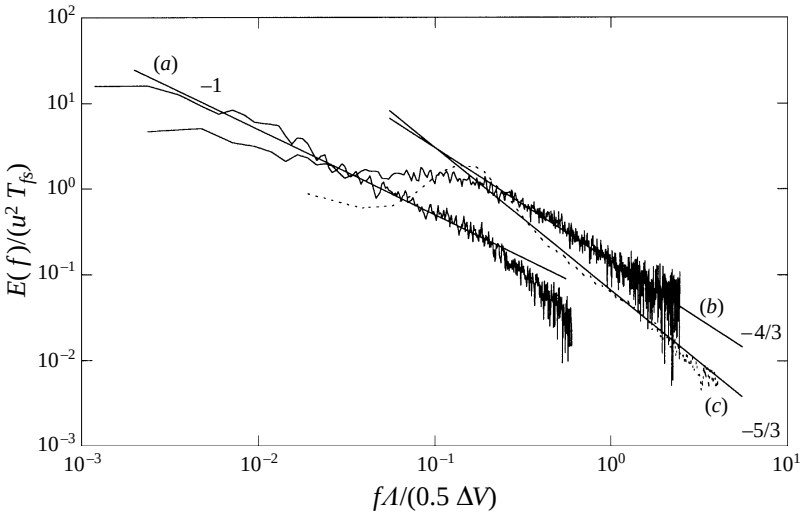

FIGURE 13. Streamwise velocity spectra at $x\}H = 2$. (*a*) $y\}H = 1.1$, (*b*) $y\}H = 1.3$, (*c*) $y\}H = 1.8$.

the Bartlett window function to reduce 'leakage' effects (Press *et al.* 1989) following Miles (1991).

To demonstrate the differences in the spectra across the flow, one-dimensional velocity spectra are shown in figure 13 for three different locations across the shear layer at $x\}H = 2$. Spectrum (*c*), taken in the free stream, clearly shows a region with a slope of $-5\}3$, corresponding to the inertial subrange. Spectra (*a*) and (*b*) were measured in the recirculation zone and in the middle of the shear layer, respectively. Neither exhibits the $-5\}3$ scaling region. The spectra are non-dimensionalized in such a way that the *y*-intercept is equal to the ratio of the local integral timescale to the free-stream integral timescale (which is estimated as the integral of the free-stream autocorrelation function to the first zero crossing). The integral timescale increases by more than an order of magnitude from the free stream to the middle of the recirculation zone.

The three positions for which spectra are shown are indicated on the turbulent kinetic energy balance in figure 11(*a*). The $-5\}3$ slope is expected in the free stream

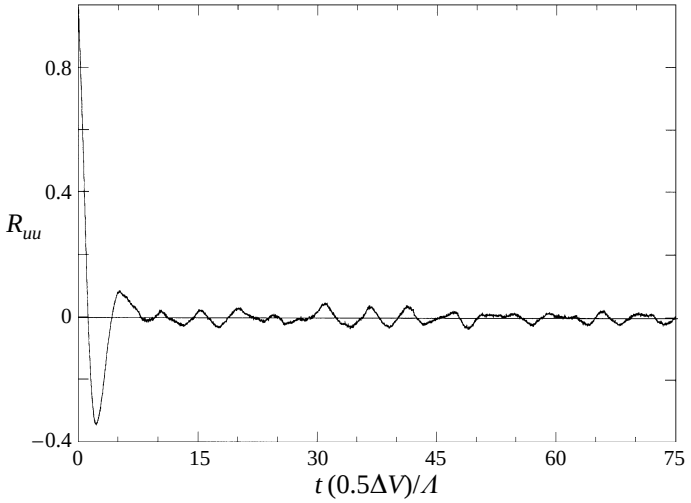

FIGURE 14. Autocorrelation function showing oscillations in the shear layer at $x\}H = 2$, $y\}H = 1.8$.

since production and dissipation are likely to be the only significant terms in the balance. As one moves into the recirculation region, where advection and turbulent transport become more important, the spectrum no longer exhibits the $-5\}3$ slope. In these regions a large portion of the turbulent kinetic energy is being transported from nearby regions where the timescales of the flow are rather different. At $y\}H = 1.1$, where the slope of the spectrum is -1, the energy is divided equally among logarithmically defined frequency bands (since $\int_0^\infty fE(f)\,\mathrm{d}\,(\ln f) = \overline{u^2}$) consistent with the idea that the flow at that point has been influenced by a range of different timescales through the transport of turbulence from non-local sources.

The autocorrelation function is shown in figure 14 for the location $x\}H = 2$, $y\}H = 1.9$, which is just at the outer edge of the shear layer fairly close to the point of separation. An oscillation is seen that persists to very long lag times (at least 100 times the integral timescale). This oscillation corresponds to the broad spectral peak at $f\Lambda\}U_{sl} = 0.2$. Vortical structures that develop in a free mixing layer have a characteristic frequency of $f\Lambda\}U_{sl} = 0.2$, where U_{sl}, the shear layer velocity, is equal to the average of the high and low mean velocities of the mixing layer (Winant & Browand 1974). This characteristic frequency is seen as a peak in the velocity spectrum measured by Driver *et al.* (1983) for the flow over a backward-facing step. Figure 15(*a*) shows both the streamwise and cross-stream velocity spectra at $x\}H = 3$ and $y\}H = 1.9$. A broad spectral peak centred at $f\Lambda\}U_{sl} = 0.2$ is observed, and can be seen in the spectra from $x\}H = 1$–4 (the frequency where the peak occurs varies between $f\Lambda\}U_{sl} = 0.2$ and 0.3, increasing gradually in the streamwise direction). For the present results, the shear layer velocity was estimated to be half the velocity difference across the shear layer.

Very low-frequency 'flapping' of the shear layer has been reported in many separated and reattaching flows (e.g. Eaton & Johnston 1982; Castro & Haque 1987; Kiya & Sasaki 1983). Castro & Haque state that this very low-frequency motion can be seen as a peak in the velocity or wall-pressure spectrum, and that the timescale which corresponds to this low-frequency motion is approximately eight times as long as a fluid particle in the free stream requires to traverse the length of the recirculation region. In the present study, the non-dimensional frequencies which correspond to this

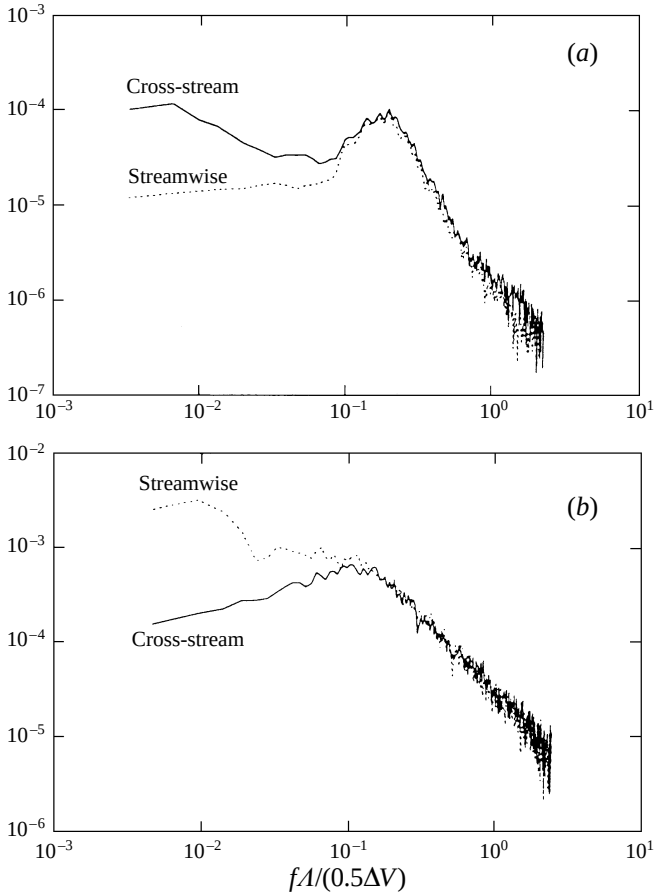

FIGURE 15. Cross-stream and streamwise velocity spectra at (*a*) $x\}H = 3$, $y\}H = 1.9$; (*b*) $x\}H = 7$, $y\}H = 1.9$.

very low-frequency motion are $f\Lambda\}U_{sl} = 0.01$ and 0.023 at $x\}H = 3$ and 7, respectively. Although there are no clear spectral peaks in figures 15(*a*) and 15(*b*), we can see that the flow contains considerable energy at these very low frequencies. At $x\}H = 3$, the cross-stream velocity spectrum has significantly more energy at these low frequencies than the streamwise spectrum, consistent with the idea of cross-stream flapping of the shear layer as discussed by Eaton & Johnston (1982). However, closer to reattachment at $x\}H = 7$, the streamwise spectrum shows more low-frequency energy than the cross-stream spectrum. Since the reattachment point is constrained to move along the wall (in the streamwise direction), it is reasonable to speculate that as reattachment is approached, the low-frequency streamwise fluctuations have more energy than the cross-stream fluctuations.

5. Conclusion

Mean velocity and Reynolds stress profiles measured using laser Doppler velocimetry were presented for the flow over a surface-mounted triangular obstacle. Derived quantities were also discussed, including momentum and turbulent kinetic energy balances, and autocorrelations and spectra. Special care was taken to avoid overestimating the turbulence quantities which are sensitive to the uncorrelated noise in the LDV signal.

The thickness of the shear layer, as measured by the vorticity thickness, grows at an almost constant rate for the forward half of the separated region. Midway between the separation point and the reattachment point a noticeable decrease in the growth rate occurs, coinciding with the loss of a distinct peak in the velocity spectrum. The spectral peak is believed to be caused by vortical structures which form in the shear layer as has been reported for the free mixing layer (Winant & Browand 1974). Future work investigating a connection between these simultaneous occurrences would be advantageous.

The flow over a surface-mounted triangular obstacle differs from the flow over a backward-facing step because of the acceleration of the flow as it passes over the obstacle and separates. The acceleration has an effect on the structure parameter $\overline{v^2}\}\overline{u^2}$ in the free stream, causing a dramatic increase before separation. Also the acceleration of the flow over the obstacle causes the boundary layer at separation to be thin relative to the obstacle height.

The momentum balances show the favourable pressure gradient produced by the acceleration of the free stream just downstream of separation and the unfavourable pressure gradient closer to reattachment that works to produce the reverse flow in the recirculation region. The cross-stream advection term behaves differently at the two locations shown because of the difference in the cross-stream flow direction.

The turbulent kinetic energy balances show a small region at the edge of the shear layer where unphysical levels of dissipation contribute to the turbulence, as seen in the separated boundary layer flow. The pressure transport term is neglected in balancing the equation to determine the dissipation rate; therefore, this may indicate the importance of pressure transport in these flows. It is also seen that streamwise advection is the major source of turbulence in the near-wall region of the recirculation zone close to separation.

The velocity spectra for this flow shows a gradual increase in slope (from $-5\}3$ to -1) between the free stream and the middle of the recirculation region. Concurrent with this increase in slope is a decrease in the role of shear production in the turbulent kinetic energy balance and an increase in the role of the advection and turbulent transport terms.

The very low-frequency motion of the shear layer is seen to contribute energy preferentially to different components of the velocity fluctuations depending on the location in the flow. Closer to the separation point there is more low-frequency energy in the cross-stream fluctuations than there is in the streamwise fluctuations, whereas closer to the reattachment point the opposite is true.

REFERENCES

Adams, E. W. & Johnston, J. P. 1988 Flow structure in the near-wall zone of a turbulent separated flow. *AIAA J.* **26**, 932–939.

Armaly, B. F., Durst, F., Pereira, J. C. F. & Schonung, B. 1983 Experimental and theoretical investigation of backward-facing step flow. *J. Fluid Mech.* **127**, 473–496.

Arya, S. P. S., Capuano, M. E. & Fagen, L. C. 1987 Some fluid modelling studies of flow and dispersion over two-dimensional low hills. *Atmos. Environ.* **21**, 753–764.

Atli, V. 1988 Subsonic flow over a two-dimensional obstacle immersed in a turbulent boundary layer on a flat surface. *J. Wind Engng Indust. Aerodyn.* **31**, 225–239.

Boston, N. E. J. & Burling, R. W. 1972 An investigation of high-wavenumber temperature and velocity spectra in air. *J. Fluid Mech.* **55**, 473–492.

Castro, I. P. 1989 *An Introduction to the Digital Analysis of Stationary Signals*. Adam Hilger}ESM.

CASTRO, I. P. & HAQUE, A. 1987 The structure of a turbulent shear layer bounding a separation region. *J. Fluid Mech.* **179**, 439–468.

CHANDRSUDA, C. & BRADSHAW, P. 1981 Turbulent structure of a reattaching mixing layer. *J. Fluid Mech.* **110**, 171–194.

DEBRODERODE, V. & BRADSHAW, P. 1972 Three-dimensional flow in nominally two-dimensional separation bubbles I. Flow behind a rearward-facing step. *Imperial College of Science and Technology, Aero. Rep.* 72–19.

DIANAT, M. & CASTRO, I. P. 1991 Turbulence in a separated boundary layer. *J. Fluid Mech.* **226**, 91–123.

DRAIN, L. E. 1980 *The Laser Doppler Technique*. John Wiley.

DRIVER, D. M. & SEEGMILLER, H. L. 1985 Feature of a reattaching turbulent shear layer in a diverging channel flow. *AIAA J.* **23**, 163–171.

DRIVER, D. M., SEEGMILLER, H. L. & MARVIN, J. G. 1983 Time dependent behavior of a reattaching shear layer. *AIAA J.* **25**, 914–919.

EATON, J. K. & JOHNSTON, J. P. 1981 A review of research on subsonic turbulent flow reattachment. *AIAA J.* **19**, 1093–1100.

EATON, J. K. & JOHNSTON, J. P. 1982 Low frequency unsteadiness of a reattaching turbulent shear layer. In *Turbulent Shear Flows 3* (ed. L. J. S. Bradbury, F. Durst, B. E. Launder, F. W. Schmidt & J. H. Whitelaw), p. 162. Springer.

HANCOCK, P. E. & CASTRO, I. P. 1993 End effects in nominally two-dimensional separated flows. In *Advances in Turbulence Research IV* (ed. F. T. M. Nieustadt), vol. 51, pp. 173–179. Applied Scientific Research.

HEIST, D. K., RAVICHANDRAN, M. & GOULDIN, F. C. 1994 Incinerator related flow – an experimental and numerical study of turbulent-flow over an obstacle. *Combust. Sci. Technol.* **101**, 425–441.

KIYA, M. & SASAKI, K. 1983 Structure of a turbulent separation bubble. *J. Fluid Mech.* **137**, 83–113.

MAYO, W. T. JR 1978 Spectrum measurements with laser velocimeters. In *Proc. Dynamic Flow Conf. Denmark*, pp. 851–868.

MEHTA, R. D. & WESTPHAL, R. V. 1986 Near-field turbulence properties of single- and two-stream plane mixing layers. *Exps. Fluids* **4**, 257–266.

MILES, P. C. 1991 Conditional velocity statistics and time-resolved flamelet statistics in premixed turbulent v-shaped flames. PhD thesis, Cornell University.

MORETTI, P. M. & KAYS, W. M. 1965 Heat transfer to a turbulent boundary layer with varying free-stream velocity and varying surface temperature – an experimental study. *Intl J. Heat Mass Transfer* **8**, 1187–1202.

PRESS, W. H., FLANNERY, B. P., TEUKOLSKY, S. A. & VETTERLING, W. T. 1989 *Numerical Recipes in PASCAL: the Art of Scientific Computing*. Cambridge University Press.

RUDERICH, R. & FERNHOLZ, H. H. 1986 An experimental investigation of a turbulent shear flow with separation, reverse flow, and reattachment. *J. Fluid Mech.* **163**, 283–322.

SIMPSON, R. L. 1981 The structure of a separating turbulent boundary layer. Part 1. Mean flow and Reynolds stresses. *J. Fluid Mech.* **113**, 23–51.

SIMPSON, R. L. 1985 Two-dimensional turbulent separated flows. *AGARDograph* 287.

STEVENSON, W. H., THOMPSON, H. D. & ROESLER, T. C. 1982 A direct measurement of laser velocimetry bias errors in a turbulent flow. *AIAA J.* **20**, 1720.

TENNEKES, H. & LUMLEY, J. L. 1972 *A First Course in Turbulence*. The MIT Press.

THANGAM, S. & SPEZIALE, C. G. 1992 Turbulent flow past a backward-facing step: a critical evaluation of two-equation models. *AIAA J.* **30**, 1314.

TOWNSEND, A. A. 1976 *The Structure of Turbulent Shear Flow*, 2nd edn. Cambridge University Press.

WESTPHAL, R. V., JOHNSTON, J. P. & EATON, J. K. 1984 Experimental study of flow reattachment in a single-sided expansion. *NASA CR*-3765.

WHIFFEN, M. C., LAU, J. C. & SMITH, D. M. 1978 Design of LV experiments for turbulence measurements. *Proc. Third Intl Workshop on Laser Velocimetry, Purdue University*, pp. 197–207.

WINANT, C. & BROWAND, F. 1974 Vortex pairing: The mechanism of turbulent mixing-layer growth at moderate Reynolds numbers. *J. Fluid Mech.* **63**, 237–255.